Spectral and Structural Variations of Biomimetic Light-Harvesting Nanotubes

Loehner, A.; Kunsel, T.; Roehr, M. I. S.; Jansen, T. L. C.; Sengupta, S.; Wuerthner, F.; Knoester, J.; Koehler, J.

Published in:
JOURNAL OF PHYSICAL CHEMISTRY LETTERS

DOI:
10.1021/acs.jpclett.9b00303

Publication date:
2019

THE JOURNAL OF PHYSICAL CHEMISTRY Letters

Letter

Cite This: J. Phys. Chem. Lett. 2019, 10, 2715−2724

pubs.acs.org/JPCL

Spectral and Structural Variations of Biomimetic Light-Harvesting Nanotubes

A. Löhner,[†,▽] T. Kunsel,[‡,▽] M. I. S. Röhr,[§,▽] T. L. C. Jansen,[‡] S. Sengupta,[§] F. Würthner,[*,§,#] J. Knoester,[*,‡] and J. Köhler[*,†,∥,⊥]

[†]Spectroscopy of Soft Matter, University of Bayreuth, Universitätsstraße 30, 94557 Bayreuth, Germany

[‡]University of Groningen, Zernike Institute for Advanced Materials, Nijenborgh 4, 9747 AG Groningen, The Netherlands

[§]Center for Nanosystems Chemistry, Universität Würzburg, Theodor-Boveri-Weg, 97074 Würzburg, Germany

[∥]Bavarian Polymer Institute, Universitätsstraße 30, 94557 Bayreuth, Germany

[#]Bavarian Polymer Institute, Theodor-Boveri-Weg, 97074 Würzburg, Germany

[⊥]Bayreuth Institute of Macromolecular Research (BIMF), University of Bayreuth, Universitätsstraße 30, 94557 Bayreuth, Germany

Supporting Information

ABSTRACT: Bioinspired, self-assembled nanotubes have been investigated by low-temperature, polarization-resolved single-tube spectroscopy. These assemblies are based on zinc chlorin monomers and are considered as model systems that resemble the secondary structural elements in the natural light-harvesting systems of green (non) sulfur bacteria. Compared to the natural systems, the spectral parameters extracted from the single-nanotube spectra feature distributions with significantly smaller widths, which is ascribed to a tremendous reduction of structural heterogeneity in the artificial systems. Employing quantum chemical molecular modeling the spectra of individual nanotubes can be explained consistently only for a molecular packing model that is fundamentally different from those considered so far for the natural systems. Subsequent theoretical simulations reveal that the remaining spectral variations between single nanotubes can be traced back to small variations of the mutual orientations of the monomer transition dipole moments that are far beyond the resolving power of high-resolution electron microscopy imaging techniques.

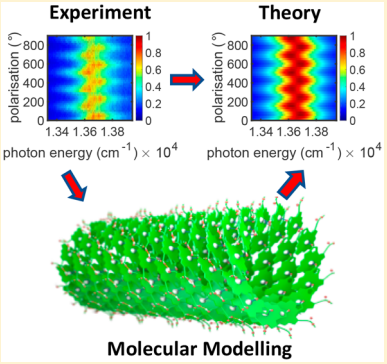

Self-assembled dye aggregates have attracted considerable attention in recent years.[1−4] In such supramolecular structures, the tight packing of the molecular building blocks results in strong intermolecular interactions that lead to the formation of exciton states, i.e., electronically excited states that are delocalized over a range of molecules and which govern essential properties, such as energy and charge transfer.[5] How and to what extent the photophysical parameters of the aggregate differ from those of the monomers depends crucially on the magnitudes of the intermolecular couplings imposed by the architecture of the supramolecular arrangement of the building blocks.[6−9]

Hence, inspired by the continuous search for novel optoelectronic materials, molecular aggregates with well-defined composition have been investigated for elucidation of the excitonic interactions in multichromophoric systems and to study their self-assembly.[3,4,10−17] Further inspiration for this research came also from the antenna complexes from green sulfur and nonsulfur bacteria, so-called chlorosomes. These belong to the most efficient light-harvesting systems in nature,[18−20] enabling photosynthetic growth by absorbing only a few photons per chromophore per day. Chlorosomes contain self-assembled molecular aggregates that accommodate hundreds of thousands of densely packed bacteriochlorophyll (BChl) *c,d,e* molecules organized in a curved lamellar or cylindrical geometry,[18,21,22] for the latter with diameters on the order of 5−10 nm and lengths in the μm range. In contrast to many other photosynthetic antenna systems, where the arrangement of the cofactors is determined by a protein scaffold, the monomers in the molecular aggregates of the chlorosomes are stabilized by metal−ligand coordinative bonds and van der Waals interactions.[19] Especially this feature has motivated many groups to investigate the design principles of chlorosomes and/or to develop synthetic analogues for next-generation solar cells.[12,23−25]

For the natural chlorosomes, the presence of mixtures of various types of BChl molecules that are involved in the self-assembly process is an important source for heterogeneity, together with variations in size, shape, and the number of aggregates in a single chlorosome. Therefore, a lot of effort has been spent synthesizing artificial bacteriochlorophyll mimics.[3,12,26] Semisynthetic 3^1-hydroxy zinc chlorin (ZnChl) molecules derived from natural chlorophyll *a* precursors are considered to be the best matching counterparts to the BChl

Received: February 1, 2019
Accepted: May 6, 2019
Published: May 6, 2019

DOI: 10.1021/acs.jpclett.9b00303
J. Phys. Chem. Lett. 2019, 10, 2715−2724

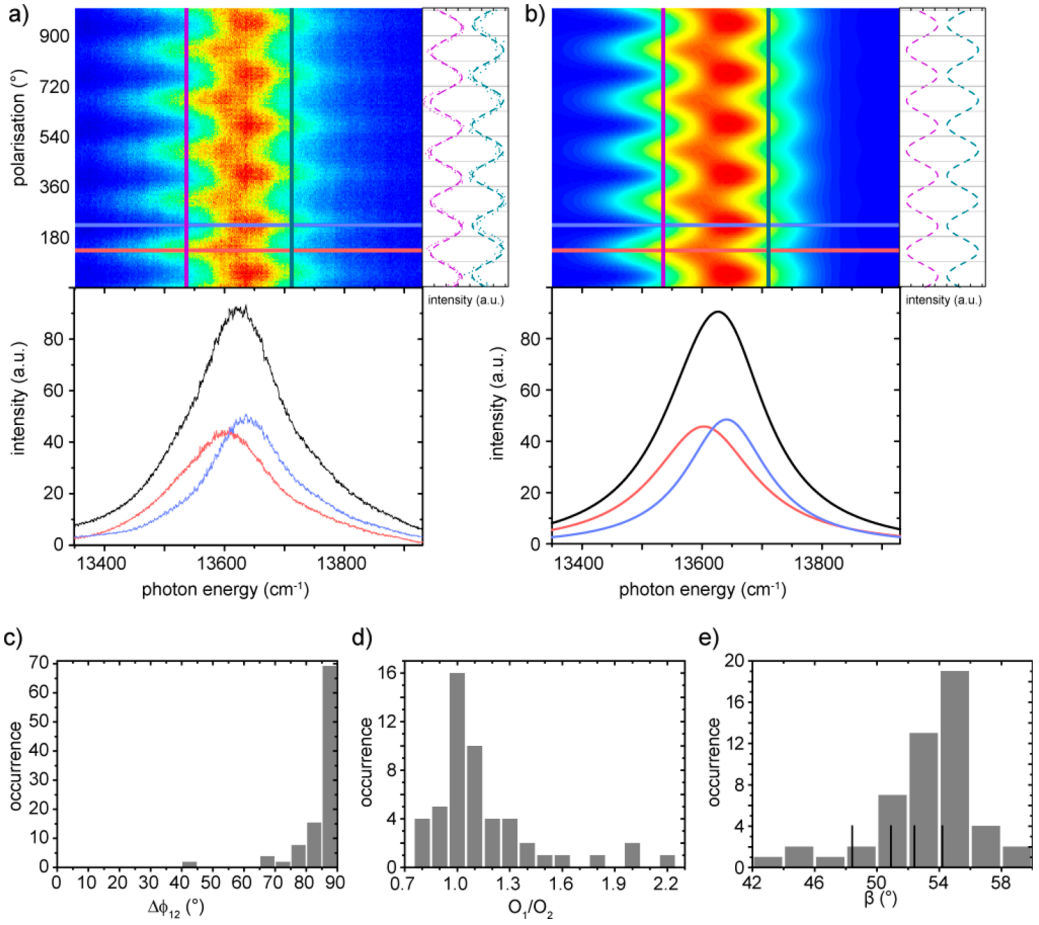

Figure 1. (a) Top: Stack of 160 consecutively recorded low-temperature fluorescence−excitation spectra from an individual aggregate of ZnChl **1**. Between two successive spectra, the polarization of the excitation has been rotated by 6.2°. On the right-hand side of the pattern, the measured fluorescence intensity (dots) is compared to a $\cos^2$ function (dashed) as a function of the polarization for excitation energies marked by the vertical solid lines at 13710 cm^{-1}/729.4 nm (dark green) and 13540 cm^{-1}/738.6 nm (pink). Bottom: Fluorescence−excitation spectrum averaged over all polarizations (black) and individual spectra at the particular polarizations of 130° (red) and 217° (blue), indicated by the respective horizontal lines in the top pattern. The excitation intensity was 25 W/cm^2. (b) Global fit of the experimental spectrum according to eq 1 (see the text). The setup of this part of the figure is similar to that in part (a). (c) Distribution of the relative phase angles between the two subbands from an individual aggregate ($\Delta\phi_{12} = |\phi_1 - \phi_2|$ if the result is less than 90° and $\Delta\phi_{12} = |180° - |\phi_1 - \phi_2||$ otherwise). (d) Distribution of the ratio of the oscillator strengths O_1/O_2 of the two subbands from an individual aggregate. (e) Experimental distribution of the angle β (gray bars) that characterizes the orientation of the transition dipole moments of the monomers with respect to the symmetry axis of a tubular aggregate. The black lines indicate the β values obtained from simulations of the four spectra shown as examples in Figure 4 (vide infra). For more details, see the text. Remark: For one single aggregate, we obtained outliers for the ratio of the oscillator strengths (5.15) and for the value of β (32°). For illustration purposes, these data points are not shown in (d) and (e), respectively.

c,*d*,*e* found in chlorosomes[3,12,24,25,27−30] because they feature a similar tetrapyrrole backbone with 3-hydroxymethyl and 13^1-keto groups as the natural BChls. Applying the concept of dendron wedges,[31] some of us accomplished the first unambiguous example of a highly defined tubular model system based on ZnChl **1**.[29] Using atomic force microscopy (AFM) and transmission electron microscopy (TEM), it was found that the ZnChl **1** monomers self-assemble into uniform single-wall tubular structures with a total diameter of 6 nm.[29] Further, the optical properties of these ZnChl **1** and related dendron-appended ZnChl aggregates[3,29,32] closely matched those of their natural counterparts.

In order to associate the geometric and the electronic structure of the ZnChl **1** aggregates, in this Letter, we combine low-temperature polarization-resolved single-molecule spectroscopy, quantum chemical structure calculations, and spectral simulations. Because the molecular composition of the monomers in ZnChl **1** aggregates is properly defined, this leads to a significant reduction of the widths of the observed spectral bands compared to those observed for single natural chlorosomes,[33−44] thereby unmasking further spectral variations between the individual ZnChl **1** aggregates. The spectral heterogeneity can be traced back to reflect subtle variations in the mutual alignment of the monomers, which are far beyond the resolving power of high-resolution imaging techniques. Interestingly, these variations can only be explained consistently if we introduce a new supramolecular stacking model between the ZnChl **1** monomers.

In Figure 1a, we display a stack of 160 consecutively recorded fluorescence−excitation spectra from a single aggregate as a function of the polarization of the incident light in a two-dimensional representation. This reveals two subbands, each showing a clear modulation of the detected fluorescence intensity with 180° periodicity, Figure 1a, top. The variation in intensity is compatible with a $\cos^2$ dependence, as indicated by the dashed lines. Integration

DOI: 10.1021/acs.jpclett.9b00303
J. Phys. Chem. Lett. 2019, 10, 2715−2724

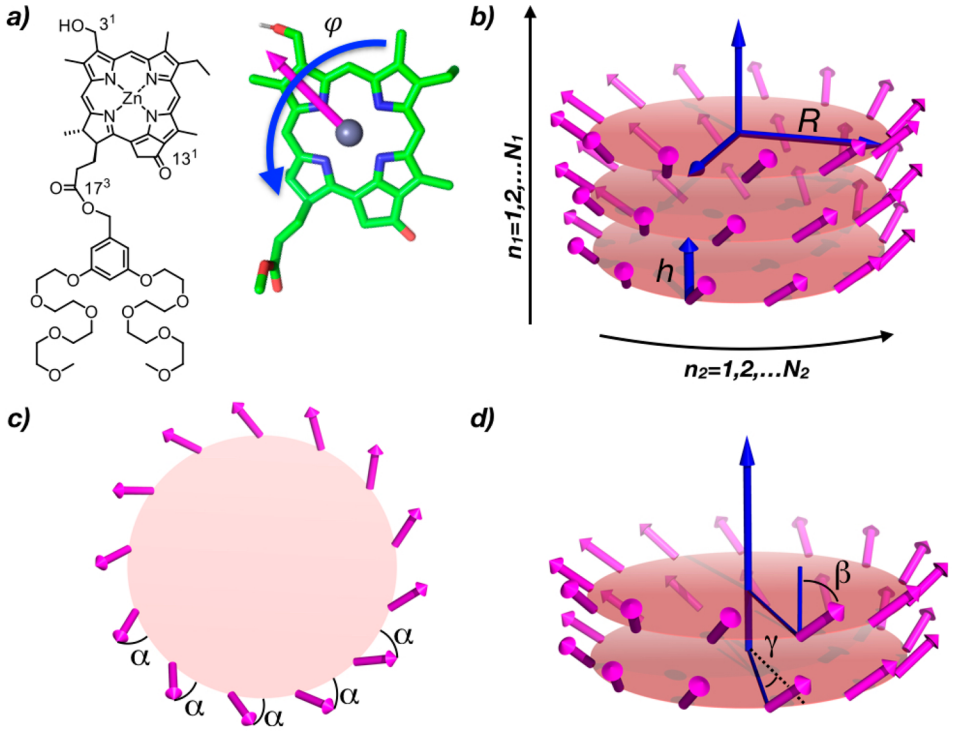

Figure 2. (a) Left: Chemical structure of the ZnChl **1** monomer. Right: Structure used for the molecular modeling. To optimize the structure, the molecule has been rotated by an angle φ (blue curved arrow) around the fixed Q_y transition dipole moment (magenta arrow). The angle φ has a value of zero when a unit vector lying in the molecular plane and perpendicular to the transition dipole moment vector is parallel to the local normal of the tube. (b) Cylindrical aggregate model composed of N_1 rings of radius R, each accommodating N_2 equidistantly arranged monomer transition dipole moments (magenta arrows). Consecutive rings are separated by distance h. (c) Top view of the cylindrical aggregate model illustrating the angle α. (d) Two consecutive rings illustrating the angles β and γ.

over all polarizations yields the spectrum shown by the black line in Figure 1a, bottom, which features a peak at 13624 cm^{-1} (734.0 nm) with a total width of 190 cm^{-1} (full width at half maximum; fwhm). The blue and red lines in Figure 1a (bottom) correspond to examples of individual spectra that have been recorded for the polarizations indicated in the two-dimensional representation by the respective horizontal lines. These are characterized by peak positions of 13604 cm^{-1} (735.1 nm) and 13641 cm^{-1} (733.1 nm) and widths (fwhm) of 204 and 168 cm^{-1}, respectively. In order to analyze the fluorescence−excitation spectra and the underlying spectral contributions more quantitatively, we used eq 1 to fit the polarization-resolved spectra.

$$F(E, \theta) = B + \sum_i A_i(E)[\cos(\theta - \phi_i)]^2 \frac{2W_i}{4(E - E_i)^2 + (W_i)^2} \quad (1)$$

Here, B accounts for a background, i counts the spectral components associated with the individual aggregate, A_i refers to the corresponding amplitude, θ is the polarization angle of the incident light, and ϕ_i represents the angle of the projection of the transition dipole vector of the respective spectral component onto the sample plane with respect to the laboratory frame. For the line shape, we assume a Lorentzian form characterized by the energetic center position E_i and a width denoted by W_i (fwhm). (Results for a Gaussian line shape function and further spectroscopic data are provided in section 1 of the SI). During the fitting process, the phases $(\theta - \phi_i)$ and the amplitudes (A_i) were treated as global parameters. It turned out that to reasonably reproduce the experimental spectra it was sufficient to restrict the analysis to two spectral components. In the following, the two spectral components, labeled as i = 1, 2, will be referred to as the low-energy (i = 1) and the high-energy band (i = 2), respectively, and the whole fitting procedure will be referred to as a *two-component fit*.

For the example shown in Figure 1a, the result of this fitting procedure is shown in Figure 1b. For the low-energy band (red line), we find a peak at 13602 cm^{-1} (735.2 nm) with a width of 210 cm^{-1} (fwhm), and for the high-energy band (blue line), the parameters are 13646 cm^{-1} (732.8 nm) for the peak position and 162 cm^{-1} for the line width. The mutual phase difference between these two bands amounts to $\Delta\phi_{12}$ = 89.0°. This global fitting procedure was used to analyze the spectra from 52 individual ZnChl aggregates, from which we extracted the mutual polarization angle, $\Delta\phi_{12}$, and the ratio of the total oscillator strengths, O_1/O_2, of the two bands. The distributions of these parameters are shown in Figure 1c,d, respectively. Further parameters such as the spectral peak positions and line widths for the low- and high-energy bands, as well as the energy difference between the peak positions of the two bands, $\Delta E = E_2 - E_1$, are provided in the SI. The relative phase angle features a narrow distribution characterized by (84 ± 8)° (mean ± standard deviation), Figure 1c, reflecting that the optical transitions that underlie the two subbands are polarized nearly perpendicular with respect to each other. For the distribution of the ratio of the oscillator strengths O_1/O_2, we find (1.23 ± 0.63), Figure 1d. The observation of a narrow distribution for the relative phase difference peaking close to 90° provides independent evidence for a tubular arrangement of the ZnChl **1** molecules, in agreement with conclusions from previous AFM and TEM experiments.[29] There it was found that the ZnChl **1** monomers self-assemble in nanotubes with

DOI: 10.1021/acs.jpclett.9b00303
J. Phys. Chem. Lett. 2019, 10, 2715−2724

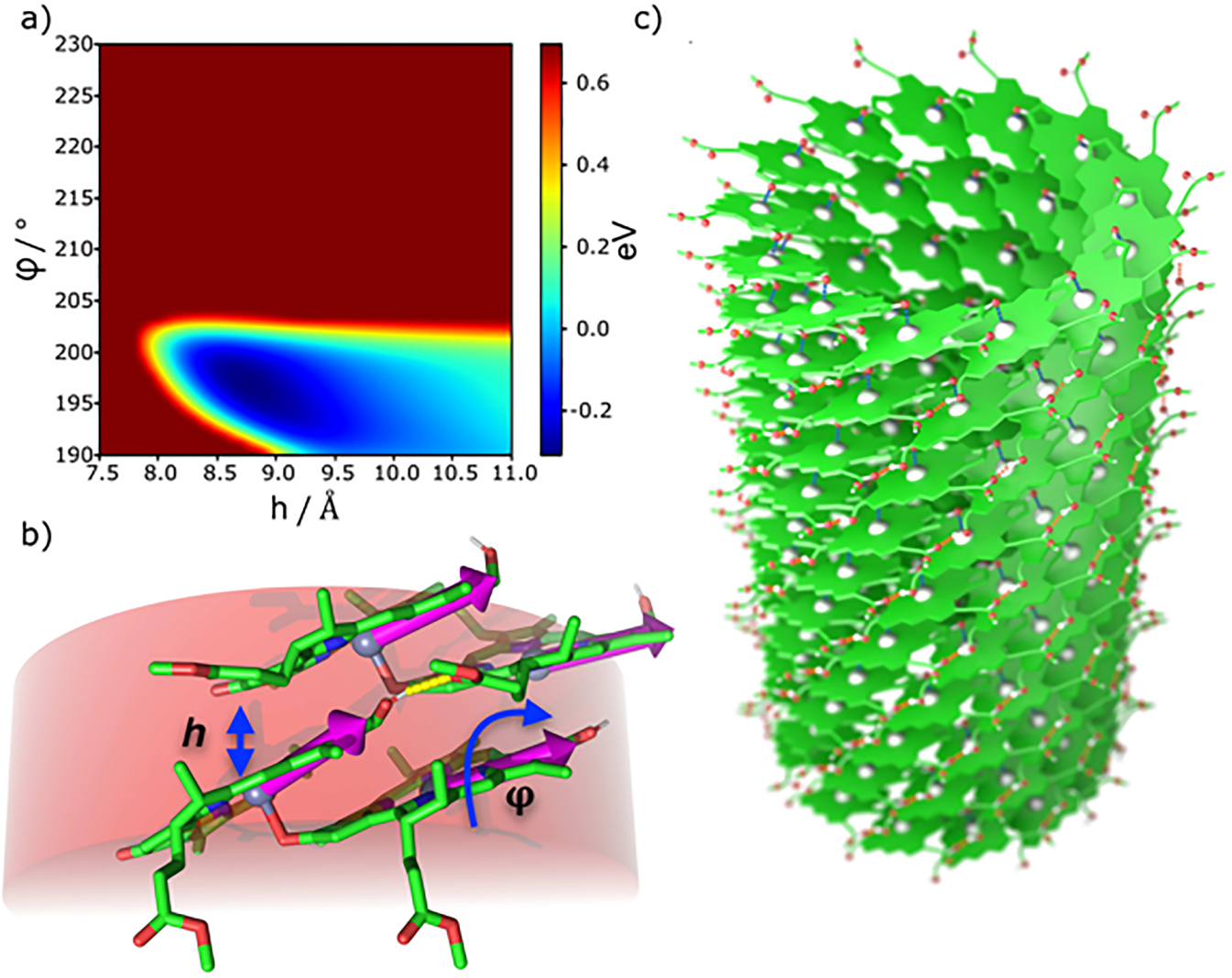

Figure 3. (a) Energy scan for $N_2 = 13$ as a function of φ and h. (b) Section consisting of four molecules from the optimized structure. The dotted yellow line corresponds to the hydrogen bond between two molecules of adjacent rings. The transition dipole moment vectors of the individual monomers are represented by magenta arrows. (c) Structural model of a tubular aggregate consisting of 10 stacked rings based on extrapolation of the optimized three-ring structure (see the text).

uniform diameter lying on the substrate with the symmetry axis parallel to the substrate. For such a sample arrangement and under the assumption of a homogeneous tubular aggregate (neither geometric nor energetic disorder), the angle β between the transition dipole moments and the cylinder axis can be calculated, in the limit of long aggregates, from the oscillator strength of the mutually orthogonally polarized bands as[6]

$$\tan(\beta) = \sqrt{\frac{2O_2}{O_1}} \tag{2}$$

Here, O_1 refers to the oscillator strength of the lower-energy exciton state, which is polarized parallel to the symmetry axis of the tube, whereas O_2 is the oscillator strength of the higher-energy exciton state that is polarized perpendicular to the symmetry axis of the tube; the factor of 2 corrects for the fact that any emission polarized parallel to the optical axis cannot be detected.[45] The experimentally obtained distribution for the angle β is shown in Figure 1e together with the results from simulations for four specific aggregates that will be discussed later. The histogram can be characterized by $(52.7 \pm 4.3)°$.

The structural information obtained from AFM or TEM is not sufficient to explain the observed variations in the angle β, which suggests differences in the molecular packing between individual aggregates that are beyond the resolving power of the high-resolution microscopies. In order to generate an atomistic model and to theoretically model the spectra of the tubular system, we have utilized the experimental information about the orientation of the transition dipole moments of individual monomers within the tube and the inner and outer tube diameters as determined previously by cryo-TEM.[29] The latter define a range for the number of ZnChl units within a cyclic/helical arrangement, and the former fix the orientation of the transition dipole moment of each individual subunit with respect to the symmetry axis of the tube. The tubular aggregates are considered as a stack of N_1 rings of radius R, each containing N_2 equidistantly arranged molecules, as illustrated in Figure 2b. In this representation, the molecules are labeled by coordinates $\mathbf{n} = (n_1,n_2)$, where n_1 runs from 1 to N_1 and labels the ring, whereas n_2 runs from 1 to N_2 and labels the position of the molecule within a particular ring. Neighboring rings are separated along the tubular axis by

DOI: 10.1021/acs.jpclett.9b00303
J. Phys. Chem. Lett. 2019, 10, 2715−2724

distance h and rotated relative to each other by the helical angle γ. For $\gamma \neq 0$, the structure of the aggregate can be envisaged as a set of helices wrapped around the same symmetry axis; see Figure 2. Then, n_2 simply numbers the helix on which each molecule lies. Thus, the three-dimensional position of molecule **n** reads[6]

$$\vec{r}_n = (R\cos(n_1\gamma + n_2\Phi_2), R\sin(n_1\gamma + n_2\Phi_2), n_1 h) \quad (3)$$

where $\Phi_2 = \frac{2\pi}{N_2}$. The orientation of the transition dipoles is characterized by the angle α between its projection on the plane of the ring and the local tangent of the ring and the angle β with respect to the cylinder axis; see Figure 2c,d. Then, the three-dimensional orientation of the molecular transition dipoles is given by

$$\vec{\mu}_n = (-\mu\sin(\beta)\sin(n_1\gamma + n_2\Phi_2 - \alpha), \mu\sin(\beta)\cos(n_1\gamma + n_2\Phi_2 - \alpha), \mu\cos(\beta)) \quad (4)$$

where μ indicates the magnitude of the transition dipole. Any tubular aggregate with one molecule per unit cell can be represented in this way. Then, the following free parameters remain to be determined: (i) the number of monomers per ring N_2, (ii) the vertical distance, h, between the two consecutive rings, and (iii) the angle of inclination, φ, of each monomer around the direction of the transition dipole moment (see Figure 2a, right).

For a systematic search of the most stable structure that obeys the given experimental constraints, we have constructed aggregates with different N_2 and systematically scanned the energy of a 2 × 2 arrangement of monomers as a function of the two undetermined parameters h and φ employing quantum chemical methodology. In this way, "Ramachandran-like" plots have been calculated from which stability regions can be identified and optimal values of the parameters h and φ can be extracted; see Figure 3a for N_2 = 13. More details and an animated movie of the structure are given in sections 2 and 3 of the SI.

In general, we found that increasing N_2 systematically leads to stable regions at higher vertical distances h. Our attempts to scan also structures for $N_2 > 16$ were not successful because for reasonable values of h the packing arrangement becomes too dense and the monomers partially overlap. This yielded unphysical structures resulting in convergence failures in the quantum chemical energy calculations. Subsequently, we extracted the structural parameters corresponding to the lowest-energy structures with N_2 ranging from 12 to 16 and constructed a minimalistic model for the tubular aggregate that consisted of two stacked rings. Then, these structures were fully relaxed, allowing us to determine the "binding energy per monomer", E_{bm}, according to

$$E_{bm} = \frac{(E_{total} - 2\cdot N_2\cdot E_{monomer})}{2\cdot N_2} \quad (5)$$

where E_{total} refers to the total energy and $E_{monomer}$ to the energy of a monomer; see Table 1.

As can be seen, the most stable configuration is obtained for the tubular structure with N_2 = 13. The corresponding energy map is shown in Figure 3a. Interestingly, already the unrelaxed structure hints toward a coordinative bond between the carbonyl group in the 13^1 position of one monomer to the Zn(II) ion of the neighboring monomer within the same ring. In the subsequently fully optimized structure, these coordination bonds become even more pronounced because the carbonyl groups bend in the direction of the neighboring metal center with a distance of 2.2 Å. Furthermore, we observe the formation of hydrogen bonds that support stacking of the individual chlorin rings. Thus, the carbonyl oxygen of the ester group coordinates with the hydroxyl group of an adjacent chlorin within the next stack with a bond length of 1.9 Å; see Figure 3b. In order to further validate the molecular arrangement found, we constructed a tubular aggregate consisting of three stacked rings according to the optimal parameters and subsequently optimized the structure, proving that in principle a periodic arrangement can be possible. The coordinative motifs are preserved in both optimized structures. In summary, the molecular modeling yields tubular aggregates that can be characterized as 13-mer ring structures held together via a metallosupramolecular Zn···O═ coordination interacting with the neighboring rings via hydrogen bonds with an offset of one monomer. In Figure 3b, a scheme illustrating the interactions between the monomers in the tube is presented. A section from the optimized structure demonstrating the binding motif is given in Figure 3c, and a comparison of the orientation of the transition dipole moments in the optimized structure with those obtained from modeling the experimentally obtained spectral patterns is given in Figure S6 in section 4 of the SI.

Table 1. Optimal Tube Parameters Calculated at the PM6-D3H4 Level[a]

N_2	h_{opt} (nm)	R_{opt} (nm)	E_{bm} (kJ/mol)
12	0.72	1.69	−30.6
13	0.67	1.69	−41.5
14	0.71	1.72	−22.0
15	1.05	1.69	−38.3
16	0.97	1.78	−34.5

[a]The parameters h_{opt} and R_{opt} were taken from the optimized structures for a system consisting of two stacked rings with variable N_2. E_{bm} represents the calculated binding energy per monomer.

The two-dimensional polarization-resolved fluorescence−excitation spectra from individual aggregates featured pronounced variations in shape; see Figure 4, left column. Yet, all patterns showed clear modulation of the registered intensity with 180° periodicities as a function of the polarization of the excitation light, and all measured spectra could be analyzed using the above-mentioned global fitting procedure. In order to investigate whether the observed spectral variations can be associated with differences in the molecular packing between the individual aggregates that are beyond the resolving power of the high-resolution imaging techniques such as electron microscopy, the spectra of the aggregates were modeled. Therefore, each monomer is represented by the transition dipole moment of the optical Q_y transition, $\vec{\mu}$, which is the only transition that is relevant for the experiments reported here. For the geometrical arrangement of the transition dipole moments, we used the parameters obtained from the molecular modeling described above as a starting point (see Table 2) and simulated the polarization-resolved fluorescence−excitation spectra of the aggregates (which are assumed to be equal to the absorption spectra) using a standard Frenkel exciton Hamiltonian that takes the excitation transfer interaction into account; see section 5 in the SI.

To fit the experimental spectra of individual nanotubes using simulations, we varied the structural parameters α, β, and γ

DOI: 10.1021/acs.jpclett.9b00303
J. Phys. Chem. Lett. 2019, 10, 2715−2724

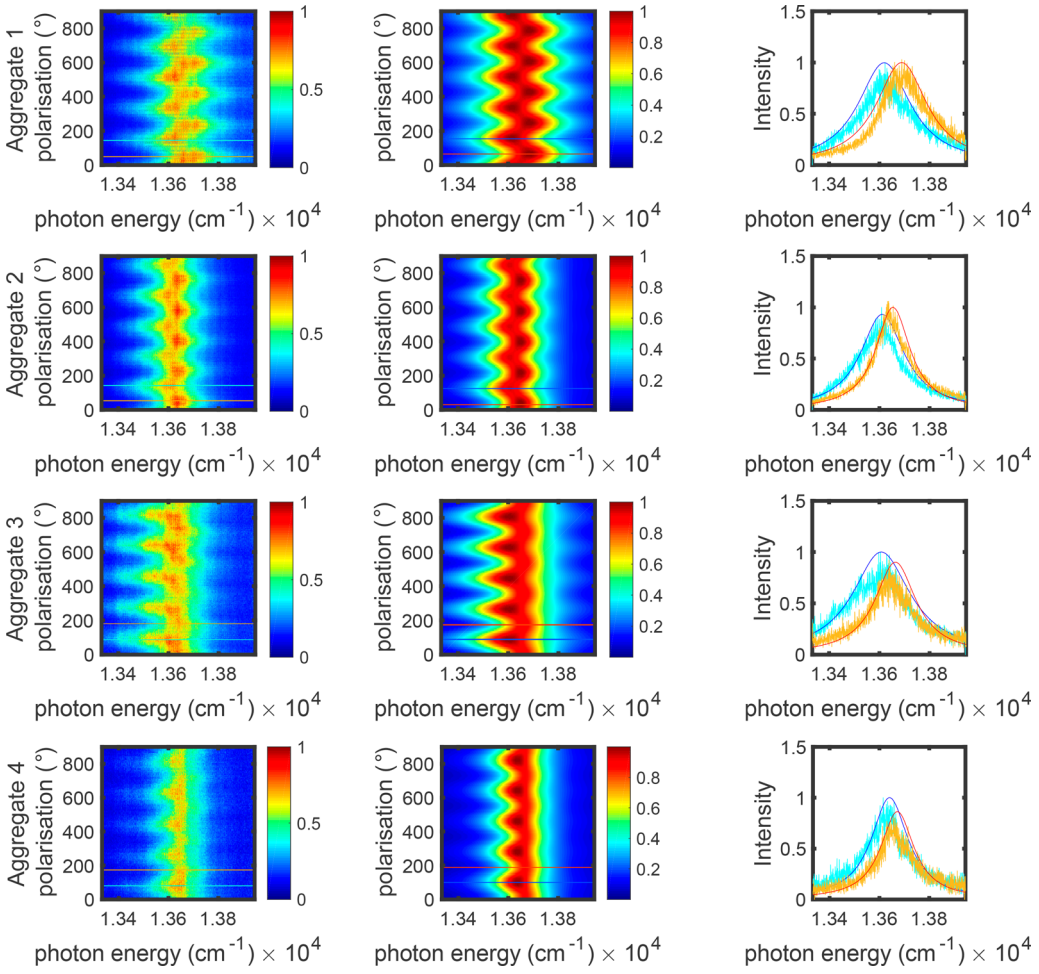

Figure 4. Left column: Examples of polarization-resolved fluorescence−excitation spectra from experiment for four different individual ZnChl **1** molecular aggregates in two-dimensional representation. The widths (fwhm) of the two spectral bands obtained from the two-component fit were (1) W_1 = 255 cm^{-1}; W_2 = 242 cm^{-1}, (2) W_1 = 210 cm^{-1}; W_2 = 162 cm^{-1}, (3) W_1 = 278 cm^{-1}; W_2 = 193 cm^{-1}, and (4) W_1 = 179 cm^{-1}; W_2 = 158 cm^{-1}. For all spectra, the excitation intensity was 25 W/cm^2. Middle column: Two-dimensional representation of simulated polarization-resolved fluorescence−excitation spectra using the structural parameters given in Table 1. The widths (fwhm) of the two spectral bands obtained from the experiment were also used in the simulated spectra to fit the experimental spectra. Right column: Comparison of cross sections through the two-dimensional representations of the experimental and the simulated spectra, allowing one to judge the quality of the fits.

Table 2. Summary of the Parameters Used for Simulating the Spectra

parameters	values
E_0	13939 cm^{-1} (717.4 nm)
μ	4.5 D
R	1.7 nm
h	0.67 nm
N_2	13
N_1	500

Table 3. Variation of the Three Angles α, β, and γ in the Simulations for Reproducing the Experimental Spectra of Aggregates 1−4 in Figure 4[a] and Comparison of the Results Obtained from the Two-Component Fit (fit) and the Spectral Simulation (sim)

	aggregate			
	1	2	3	4
α	39.9°	41.5°	40.5°	42.4°
β	54.2°	52.4°	48.4°	51.2°
γ	10°	9°	14°	10.5°
ΔE_{fit}	70 cm^{-1}	44 cm^{-1}	57 cm^{-1}	32 cm^{-1}
ΔE_{sim}	70 cm^{-1}	43 cm^{-1}	57 cm^{-1}	32 cm^{-1}
$(O_1/O_2)_{fit}$	1.000	1.146	1.487	1.270
$(O_1/O_2)_{sim}$	1.017	1.143	1.485	1.273

[a]The line widths of the two spectral bands that have been used for the simulations, W_1 and W_2, have been taken from the corresponding experimental spectra.

around the values obtained from molecular modeling. Yet, we note that within each aggregate these three angles were kept fixed, which corresponds to the situation of a totally cylindrically symmetric structure. The best agreement between each of the four experimental spectra considered, Figure 4, left column, and the corresponding modeled spectra, as shown in Figure 4, middle column, was achieved by using the parameters given in Table 3. The quality of the simulation can be judged from the comparison of slices from the 2D spectra from experiment and the model, as shown in Figure 4, right column. This can be further quantified by comparing the energetic separations $\Delta E = E_2 - E_1$ and the ratio of the oscillator strength of the two mutually perpendicular bands O_1/O_2 from the two-component fit and from the simulations; see Table 3.

DOI: 10.1021/acs.jpclett.9b00303
J. Phys. Chem. Lett. 2019, 10, 2715−2724

The numbers obtained from the fit and the simulations are in excellent agreement.

For comparison, the results of the simulations for the angle β are indicated in the experimental histogram, Figure 1e, by the black lines, confirming the good match between simulation and experiment.

For all ZnChl **1** aggregates studied, the fluorescence−excitation spectra can be decomposed into two spectral bands with mutually orthogonal polarization. This is consistent with the organization of the ZnChl **1** monomers in single-wall tubular structures, as found in the AFM and TEM experiments.[29] However, we find considerable variations between the spectral profiles of individual aggregates. These can be well understood using a tubular homogeneous model with very small variations (a few degrees) in the three angles that define the packing of the molecules within the aggregate. Intuitively, the small variations in the angles ($39.9° \leq \alpha \leq 42.4°$, $48.4° \leq \beta \leq 54.2°$, $9° \leq \gamma \leq 14°$), which cannot be resolved by high-resolution imaging techniques, seem to be acceptable from a chemical point of view to yield aggregates with the same overall morphology, in particular, with the same radius. This is also reflected by the minor variations of the corresponding lattices that underlie the tubular structures (see Figure S7 in section 4 of the SI) featuring an angle of inclination between the two lattice parameters that ranges from 58.5 to 68.5°. These values are remarkably close to the value of 58° (i.e., 180−122°) that has been proposed for the molecular arrangement of the BChl molecules within the secondary structures of the natural chlorosomes.[46]

Commonly, details of the molecular packing of the self-assembled aggregates are investigated using molecular modeling. This is a challenging task, not only due to the size of the systems but also due to the need to properly account for weak intermolecular interactions that are responsible for the structural arrangement of the (tubular) assemblies. Furthermore, the potential energy landscapes of supramolecular systems exhibit a high complexity, allowing for kinetic trapping of numerous possible structures. Usually, the modeling of tubular aggregates has been carried out either by a full quantum chemical treatment of relatively small structural models representing cut-outs of the tubular architecture[47] or by classical force field modeling[48,49] that allows for the description of substantially larger systems, but it also bears several weaknesses. First of all, standard force fields are often insufficient in the description of metallosupramolecular interactions, in particular, when transition metals are involved.[50] On the other hand, the outcome of classical modeling is strongly dependent on the parametrization. In this context, the transition metal atoms are particularly challenging for force field parametrization because they may assume different coordination numbers in different environments.

In 1994, an intriguing model based on simple semiempirical AM1 calculations was provided by Holzwarth and Schaffner. In their model, parallel metallosupramolecular stacks were interconnected by hydrogen bonds between the hydroxy and the keto groups, and the tube diameter was a function of the rotational displacement between the individual stacks.[51] However, this model cannot be reconciled with our data from single-molecule spectroscopy. Therefore, in this work, we employed an efficient quantum chemical methodology based on the semiempirical PM6-D3H4 as well as dispersion-corrected tight-binding density functional theory (DFTB) that has been proven to reliably describe the coordination environment of zinc in biological systems.[52] Using DFTB, we were able to fully optimize structures of tubular aggregates containing 39 individual ZnChl monomers. This resulted in a structural model that was fundamentally different from those previously considered for the natural counterparts of our ZnChl **1** dyes, i.e., bacteriochlorophyll *c,d,e* assemblies in the chlorosomes of green (sulfur) bacteria. Thus, in our model, the dyes are organized in a cyclic array, directed by interactions between the central zinc metal ion and the keto groups (metallosupramolecular interaction) and dispersion interactions between the tetrapyrrole scaffolds ($\pi-\pi$ interactions). Further, the individual rings are interconnected with each other by hydrogen bonds between the hydroxy and the carbonyl groups of the ester functionalities. In fact, an early infrared study by Krasnovskii and co-workers[53] indeed considered the ligation of the 13^1 keto group to the central metal ion of the tetrapyrrole ring (there Mg; in our case Zn) but was afterward replaced by models that favored coordination of the hydroxy group to the central metal in either so-called parallel and antiparallel arrangement, as suggested for the first time by Smith and Kerres.[54]

At the moment, it is not clear whether this newly suggested molecular packing for the ZnChl **1** aggregates is also of relevance for the natural chlorosomes. Yet, it is obvious that for the ZnChl **1** aggregates the distributions of the spectral parameters extracted from the spectra are clearly narrower with respect to the corresponding distributions obtained from the natural chlorosomes.[43,44] This suggests a more homogeneous supramolecular structure for the synthetic system. Presumably, this reflects that in the synthetic system the type of monomeric building block is perfectly controlled. Thus, it consists of a specific chlorin π-scaffold, a particular solubilizing side chain, and is a single stereoisomer, whereas the various types of BChl *c,d,e* molecules that are co-self-assembled in the natural chlorosomes are inhomogeneous with regard to the π-core, the side chains, and the stereochemistry at the 3^1 position, giving rise to a more disordered molecular arrangement.[46] The interpretation that the structural order of the aggregates is closely related to the diversity (or the lack thereof) of the molecular building blocks is supported by data obtained from single chlorosomes from mutated species.[43,44]

In contrast to what has been found for single natural chlorosomes, the width of the low-energy band exceeds that of the high-energy band for most of the ZnChl **1** aggregates. This cannot be explained by an additional relaxation channel for the higher energetic state, for example, a decay to the low-energy state, because this would yield exactly the opposite result. This finding is a strong indication that the observed bands are still inhomogeneously broadened. Given the soft structure of the assemblies, it is reasonable to consider slight structural variations in the overall arrangement of the ZnChl **1** monomers with respect to the symmetry axis of the overall structure within a single aggregate that are beyond the resolving power of high-resolution imaging microscopies. Further studies will be needed to shed more light on this issue.

MATERIALS AND METHODS

Sample Preparation for Single Particle Spectroscopy. The ZnChl **1** aggregates were prepared as previously reported[29] and stored in a methanol/water (1:100; vol/vol) solution at room temperature in the dark until they were used. AFM and STEM images (see ref 30 and section 6 of the SI) demonstrate that isolated nanotubes are present at concentrations below

DOI: 10.1021/acs.jpclett.9b00303
J. Phys. Chem. Lett. 2019, 10, 2715−2724

0.01 mM in methanol/water (1:100; vol/vol); see Figure S8. For the single-particle experiments, the ZnChl **1** solution was diluted in two steps with a 1% THF aqueous solution to a concentration in the nanomolar (nM) range for the ZnChl **1** aggregates. During the second dilution step, the sample solution was mixed in a 1:4 ratio (vol/vol) with a 1% THF aqueous solution that contained in addition 2 g of poly(vinyl alcohol) per 100 mL. From this mixture 15 μL were spread on a clean SiO_2 substrate and adsorbed for 2 min under nitrogen atmosphere. Subsequently, it was spin-coated at 500 rpm for 20 s, followed by 2000 rpm for 60 s. This procedure resulted in a film with a thickness of less than 1 μm that contained immobilized, well-separated single aggregates. Next, the sample was mounted in the dark in a sample holder that was inserted quickly into a precooled (77 K) bath cryostat, which allowed cooling down the samples to 1.2 K.

Fluorescence–Excitation Spectroscopy. To select a single aggregate, the sample was excited at 735 nm with the output from a Titan-Sapphire laser (3900S, Spectra Physics) that was pumped by a Nd:YVO_4 laser (Millenia Vs, Spectra Physics). The excitation light passed a home-built microscope that could be operated in wide-field mode to locate the nanotubes or confocal mode to take the fluorescence–excitation spectra. The emission from the single complexes was collected by a microscope objective (Mikrothek, NA = 0.85) mounted inside of the cryostat, transmitted through two long-pass filters (LP780, AHF Analysetechnik), and detected with a CCD camera (iKon, Andor) in wide-field mode (see Figure S9 in section 7 of the SI) or a single-photon counting avalanche photodiode (APD) (SPCM-AQR-16, PerkinElmer) in confocal mode. A fluorescence–excitation spectrum was obtained by varying the excitation wavelength between 717 and 750 nm by rotating a birefringent filter with a stepper motor (Actuator 850F, Motion Controller MM4005, Newport) in the laser cavity. Between two successive laser scans, the polarization of the excitation light was rotated by 6.2° by turning the $\lambda/2$ waveplate with a stepper motor (Owis GmbH). The excitation intensity was 25 W/cm^2, and all experiments were conducted at 1.2 K. A more detailed description in provided is section 7 of the SI.

Molecular Modeling. The initial structures of the tubular aggregates were generated by placing the monomers along the tube, such that the orientation of the transition dipole moments was consistent with the experimental data. For this purpose, the same model was used as for the simulation of the spectra (vide infra). Subsequently, the tubular aggregate was optimized using the semiempirical PM6 method[55] together with an appropriate dispersion correction and description of hydrogen bonds (D3H4) as implemented in the MOPAC package.[56] The structures were further refined by using DFTB[57−60] along with the appropriate dispersion correction[61] as implemented in the "DFTB+" program package.[62] Notice that in the molecular structure of the monomers the benzyl group bearing oligoethyleneglycol chains has been replaced by a methyl group for simplification of calculations.

Spectral Simulation Method. The polarization-resolved spectra were simulated for homogeneous tubular molecular aggregates using as a starting point the orientations of the monomer transition dipole moments as obtained from the molecular modeling. When fitting to the polarization-dependent spectra of individual aggregates, these angles were slightly varied. The eigenstates (exciton states) and energies of the electronic states of the entire aggregates were obtained by diagonalizing a standard Frenkel exciton Hamiltonian using ref 63 (see also section 5 of the SI). Using the thus obtained exciton energies and corresponding oscillator strengths, a stick spectrum was created based on Fermi's golden rule. For each single aggregate, the final spectra were then obtained by convolution of the stick spectra with Lorentzian functions with full widths at half-maxima that were adjusted manually for best match with the experimental spectra. More details are provided in the Supporting Information.

■ ASSOCIATED CONTENT

Supporting Information

The Supporting Information is available free of charge on the ACS Publications website at DOI: 10.1021/acs.jpclett.9b00303.

Further distributions of spectral parameters, molecular modelling, transition dipole moments and lattice structures, spectral simulation, scanning transmission electron microscopy (STEM) of ZnChl aggregates, and optical selection of single nanotubes (PDF)

Animated movie of the optimized structure (MPG)

■ AUTHOR INFORMATION

ORCID

A. Löhner: 0000-0003-1883-6538
M. I. S. Röhr: 0000-0002-2128-3498
T. L. C. Jansen: 0000-0001-6066-6080
F. Würthner: 0000-0001-7245-0471
J. Köhler: 0000-0002-4214-4008

Author Contributions

[▽]A.L., T.K., and M.I.S.R. contributed equally to this work. A.L. conducted single-molecule experiments, T.K. performed spectral simulations and cowrote the paper, M.I.S.R. performed molecular structure calculations and cowrote the paper, T.L.C.J. supervised spectral simulations and cowrote the paper, S.S. performed chemical synthesis, F.W. supervised chemical synthesis and cowrote the paper, J. Knoester supervised spectral simulations and cowrote the paper, and J. Köhler supervised optical experiments and wrote the paper.

Notes

The authors declare no competing financial interest.

■ ACKNOWLEDGMENTS

We thank Dr. Vladimir Stepanenko (Würzburg) for STEM measurements. Financial support from the German Science Foundation (DFG, A.L., J. Köhler: GRK 1640), the State of Bavaria in the framework of the Collaborative Research Network "Solar Technologies go Hybrid" (A.L., J. Köhler, M.I.S.R., F.W.), the Elite Network of Bavaria (ENB) program "Macromolecular Science" (J. Köhler), and the Bavarian Polymer Institute (BPI, KeyLabs for Electron and Optical Microscopy and for Supramolecular Polymers; A.L., J. Köhler, F.W.) is gratefully acknowledged.

■ REFERENCES

(1) Würthner, F.; Kaiser, T. E.; Saha-Möller, C. R. J-aggregates: from serendipitous discovery to supramolecular engineering of functional dye materials. *Angew. Chem. Int. Edit* **2011**, *50*, 3376−3410.

(2) Haedler, A. T.; Kreger, K.; Issac, A.; Wittmann, B.; Kivala, M.; Hammer, N.; Köhler, J.; Schmidt, H.-W.; Hildner, R. Long-range energy transport in single supramolecular nanofibres at room temperature. *Nature* **2015**, *523*, 196−199.

DOI: 10.1021/acs.jpclett.9b00303
J. Phys. Chem. Lett. 2019, 10, 2715−2724

(3) Balaban, S.; Tamiaki, H.; Holzwarth, A. R. Chlorins Programmed for Self-Assembly. In *Supermolecular Dye Chemistry*; Würthner, F., Ed.; Springer Verlag: Berlin, Heidelberg, 2005; Vols. *258*, pp 1−38.
(4) Eisele, D. M.; Arias, D. H.; Fu, X.; Bloemsma, E. A.; Steiner, C. P.; Jensen, R. A.; Rebentrost, P.; Eisele, H.; Tokmakoff, A.; Lloyd, S.; Nelson, K. A.; Nicastro, D.; Knoester, J.; Bawendi, M. G. Robust excitons inhabit soft supramolecular nanotubes. *Proc. Natl. Acad. Sci. U. S. A.* **2014**, *111*, E3367−75.
(5) Brixner, T.; Hildner, R.; Köhler, J.; Lambert, C.; Würthner, F. Exciton Transport in Molecular Aggregates - From Natural Antennas to Synthetic Chromophore Systems. *Adv. Energy Mater.* **2017**, *7*, 1700236.
(6) Didraga, C.; Klugkist, J. A.; Knoester, J. Optical Properties of Helical Cylindrical Molecular Aggregates: The Homogeneous Limit. *J. Phys. Chem. B* **2002**, *106*, 11474−11486.
(7) Knoester, J.; Agranovich, V. M. Frenkel and Charge-Transfer Excitons in Organic Solids. In *Electronic excitations in organic based nanostructures*; Bassani, F. G., Agranovich, V. M., Eds.; Elsevier: Amsterdam, The Netherlands, 2003; Vols. *31*, pp 1−96.
(8) Spano, F. C. The Spectral Signatures of Frenkel Polarons in H- and J-Aggregates: Accounts of Chemical Research. *Acc. Chem. Res.* **2010**, *43*, 429−439.
(9) Hestand, N. J.; Spano, F. C. Molecular Aggregate Photophysics beyond the Kasha Model: Novel Design Principles for Organic Materials. *Acc. Chem. Res.* **2017**, *50*, 341−350.
(10) Scheblykin, I. G.; Sliusarenko, O. Y.; Lepnev, L. S.; Vitukhnovsky, A. G.; van der Auweraer, M. Excitons in Molecular Aggregates of 3,3′-Bis-[3-sulfopropyl]-5,5′-dichloro-9- ethylthiacarbocyanine (THIATS): Temperature Dependent Properties. *J. Phys. Chem. B* **2001**, *105*, 4636−4646.
(11) Saer, R. G.; Blankenship, R. E. Light harvesting in phototrophic bacteria: Structure and function. *Biochem. J.* **2017**, *474*, 2107−2131.
(12) Sengupta, S.; Würthner, F. Chlorophyll J-Aggregates: From Bioinspired Dye Stacks to Nanotubes, Liquid Crystals, and Biosupramolecular Electronics. *Acc. Chem. Res.* **2013**, *46*, 2498−2512.
(13) Lang, E.; Sorokin, A.; Drechsler, M.; Malyukin, Y. V.; Köhler, J. Optical spectroscopy on individual amphi-PIC J-aggregates. *Nano Lett.* **2005**, *5*, 2635−2640.
(14) Kaiser, T. E.; Scheblykin, I. G.; Thomsson, D.; Würthner, F. Temperature-dependent exciton dynamics in J-aggregates-when disorder plays a role. *J. Phys. Chem. B* **2009**, *113*, 15836−15842.
(15) Wan, Y.; Stradomska, A.; Fong, S.; Guo, Z.; Schaller, R. D.; Wiederrecht, G. P.; Knoester, J.; Huang, L. Exciton Level Structure and Dynamics in Tubular Porphyrin Aggregates. *J. Phys. Chem. C* **2014**, *118*, 24854−24865.
(16) Eisele, D. M.; Knoester, J.; Kirstein, S.; Rabe, J. P.; Vanden Bout, D. A. Uniform exciton fluorescence from individual molecular nanotubes immobilized on solid substrates. *Nat. Nanotechnol.* **2009**, *4*, 658−663.
(17) Eisele, D. M.; Cone, C. W.; Bloemsma, E. A.; Vlaming, S. M.; van der Kwaak, C. G. F.; Silbey, R. J.; Bawendi, M. G.; Knoester, J.; Rabe, J. P.; Vanden Bout, D. A. Utilizing redox-chemistry to elucidate the nature of exciton transitions in supramolecular dye nanotubes. *Nat. Chem.* **2012**, *4*, 655−662.
(18) Oostergetel, G. T.; van Amerongen, H.; Boekema, E. J. The chlorosome: a prototype for efficient light harvesting in photosynthesis. *Photosynth. Res.* **2010**, *104*, 245−255.
(19) Blankenship, R. E.; Matsuura, K. Antenna Complexes from Green Photosynthetic Bacteria. In *Light-Harvesting Antennas in Photosynthesis*; Green, B. R., Parson, W. W., Eds.; Springer Netherlands: Dordrecht, The Netherlands, 2003.
(20) Beatty, J. T.; Overmann, J.; Lince, M. T.; Manske, A. K.; Lang, A. S.; Blankenship, R. E.; van Dover, C. L.; Martinson, T. A.; Plumley, F. G. An obligately photosynthetic bacterial anaerobe from a deep-sea hydrothermal vent. *Proc. Natl. Acad. Sci. U. S. A.* **2005**, *102*, 9306−9310.
(21) Alster, J.; Kabeláč, M.; Tuma, R.; Pšenčík, J.; Burda, J. V. Computational study of short-range interactions in bacteriochlorophyll aggregates. *Comput. Theor. Chem.* **2012**, *998*, 87−97.
(22) Oostergetel, G. T.; Reus, M.; Gomez Maqueo Chew, A.; Bryant, D. A.; Boekema, E. J.; Holzwarth, A. R. Long-range organization of bacteriochlorophyll in chlorosomes of Chlorobium tepidum investigated by cryo-electron microscopy. *FEBS Lett.* **2007**, *581*, 5435−5439.
(23) Balaban, T. S. Tailoring Porphyrins and Chlorins for Self-Assembly in Biomimetic Artificial Antenna Systems. *Acc. Chem. Res.* **2005**, *38*, 612−623.
(24) Ogi, S.; Grzeszkiewicz, C.; Würthner, F. Pathway complexity in the self-assembly of a zinc chlorin model system of natural bacteriochlorophyll J-aggregates. *Chem. Sci.* **2018**, *9*, 2768−2773.
(25) Miyatake, T.; Yamamoto, Y.; Tamiaki, H. Temperature-dependent self-assemblies of zinc 3 1 -hydroxy-chlorins in polydimethylsiloxane oil. *J. Photochem. Photobiol., A* **2018**, *353*, 654−660.
(26) Otsuki, J. Supramolecular approach towards light-harvesting materials based on porphyrins and chlorophylls. *J. Mater. Chem. A* **2018**, *6*, 6710−6753.
(27) Huber, V.; Katterle, M.; Lysetska, M.; Würthner, F. Reversible self-organization of semisynthetic zinc chlorins into well-defined rod antennae. *Angew. Chem., Int. Ed.* **2005**, *44*, 3147−3151.
(28) Shoji, S.; Ogawa, T.; Hashishin, T.; Ogasawara, S.; Watanabe, H.; Usami, H.; Tamiaki, H. Nanotubes of Biomimetic Supramolecules Constructed by Synthetic Metal Chlorophyll Derivatives. *Nano Lett.* **2016**, *16*, 3650−3654.
(29) Sengupta, S.; Ebeling, D.; Patwardhan, S.; Zhang, X.; von Berlepsch, H.; Böttcher, C.; Stepanenko, V.; Uemura, S.; Hentschel, C.; Fuchs, H.; Grozema, F. C.; Siebbeles, L. D. A.; Holzwarth, A. R.; Chi, L.; Würthner, F. Biosupramolecular nanowires from chlorophyll dyes with exceptional charge-transport properties. *Angew. Chem. Int. Edit* **2012**, *51*, 6378−6382.
(30) Tamiaki, H.; Wada, A.; Matsubara, S. 20-Substitution effect on self-aggregation of synthetic zinc bacteriochlorophyll- d analogs. *J. Photochem. Photobiol., A* **2018**, *353*, 581−590.
(31) Rosen, B. M.; Wilson, C. J.; Wilson, D. A.; Peterca, M.; Imam, M. R.; Percec, V. Dendron-mediated self-assembly, disassembly, and self-organization of complex systems. *Chem. Rev.* **2009**, *109*, 6275−6540.
(32) Ganapathy, S.; Sengupta, S.; Wawrzyniak, P. K.; Huber, V.; Buda, F.; Baumeister, U.; Würthner, F.; de Groot, H. J. M. Zinc chlorins for artificial light-harvesting self-assemble into antiparallel stacks forming a microcrystalline solid-state material. *Proc. Natl. Acad. Sci. U.S.A.* **2009**, *106*, 11472−11477.
(33) Saga, Y.; Tamiaki, H.; Shibata, Y.; Itoh, S. Excitation energy transfer in individual light-harvesting chlorosome from green photosynthetic bacterium Chloroflexus aurantiacus at cryogenic temperature. *Chem. Phys. Lett.* **2005**, *409*, 34−37.
(34) Saga, Y.; Wazawa, T.; Ishii, Y.; Yanagida, T.; Tamiaki, H. Single Supramolecule Spectroscopy of Natural and Alkaline-Treated Chlorosomes from Green Sulfur Photosynthetic Bacteria. *J. Nanosci. Nanotechnol.* **2006**, *6*, 1750−1757.
(35) Shibata, Y.; Saga, Y.; Tamiaki, H.; Itoh, S. Low-Temperature Fluorescence from Single Chlorosomes, Photosynthetic Antenna Complexes of Green Filamentous and Sulfur Bacteria. *Biophys. J.* **2006**, *91*, 3787−3796.
(36) Shibata, Y.; Saga, Y.; Tamiaki, H.; Itoh, S. Polarized fluorescence of aggregated bacteriochlorophyll c and baseplate bacteriochlorophyll a in single chlorosomes isolated from Chloroflexus aurantiacus. *Biochemistry* **2007**, *46*, 7062−7068.
(37) Shibata, Y.; Saga, Y.; Tamiaki, H.; Itoh, S. Anisotropic distribution of emitting transition dipoles in chlorosome from Chlorobium tepidum: fluorescence polarization anisotropy study of single chlorosomes. *Photosynth. Res.* **2009**, *100*, 67−78.
(38) Tian, Y.; Camacho, R.; Thomsson, D.; Reus, M.; Holzwarth, A. R.; Scheblykin, I. G. Organization of Bacteriochlorophylls in Individual Chlorosomes from Chlorobaculum tepidum Studied by 2-Dimensional Polarization Fluorescence Microscopy. *J. Am. Chem. Soc.* **2011**, *133*, 17192−17199.

DOI: 10.1021/acs.jpclett.9b00303
J. Phys. Chem. Lett. 2019, 10, 2715−2724

(39) Furumaki, S.; Vacha, F.; Habuchi, S.; Tsukatani, Y.; Bryant, D. A.; Vacha, M. Absorption linear dichroism measured directly on a single light-harvesting system: the role of disorder in chlorosomes of green photosynthetic bacteria. *J. Am. Chem. Soc.* **2011**, *133*, 6703−6710.
(40) Furumaki, S.; Yabiku, Y.; Habuchi, S.; Tsukatani, Y.; Bryant, D. A.; Vacha, M. Circular Dichroism Measured on Single Chlorosomal Light-Harvesting Complexes of Green Photosynthetic Bacteria. *J. Phys. Chem. Lett.* **2012**, *3*, 3545−3549.
(41) Jendrny, M.; Aartsma, T. J.; Köhler, J. Fluorescence Excitation Spectra from Individual Chlorosomes of the Green Sulfur Bacterium Chlorobaculum tepidum. *J. Phys. Chem. Lett.* **2012**, *3*, 3745−3750.
(42) Jendrny, M.; Aartsma, T. J.; Köhler, J. Insights into the excitonic states of individual chlorosomes from Chlorobaculum tepidum. *Biophys. J.* **2014**, *106*, 1921−1927.
(43) Günther, L. M.; Jendrny, M.; Bloemsma, E. A.; Tank, M.; Oostergetel, G. T.; Bryant, D. A.; Knoester, J.; Köhler, J. Structure of Light-Harvesting Aggregates in Individual Chlorosomes. *J. Phys. Chem. B* **2016**, *120*, 5367−5376.
(44) Günther, L. M.; Löhner, A.; Reiher, C.; Kunsel, T.; Jansen, T. L. C.; Tank, M.; Bryant, D. A.; Knoester, J.; Köhler, J. Structural Variations in Chlorosomes from Wild-Type and a bchQR Mutant of Chlorobaculum tepidum Revealed by Single-Molecule Spectroscopy. *J. Phys. Chem. B* **2018**, *122*, 6712−6723.
(45) Kang, H.; Jia, B.; Gu, M. Polarization characterization in the focal volume of high numerical aperture objectives. *Opt. Express* **2010**, *18*, 10813−10821.
(46) Ganapathy, S.; Oostergetel, G. T.; Wawrzyniak, P. K.; Reus, M.; Gomez Maqueo Chew, A.; Buda, F.; Boekema, E. J.; Bryant, D. A.; Holzwarth, A. R.; de Groot, H. J. M. Alternating syn-anti bacteriochlorophylls form concentric helical nanotubes in chlorosomes. *Proc. Natl. Acad. Sci. U.S.A.* **2009**, *106*, 8525−8530.
(47) Pandit, A.; Ocakoglu, K.; Buda, F.; van Marle, T.; Holzwarth, A. R.; de Groot, H. J. M. Structure determination of a bio-inspired self-assembled light-harvesting antenna by solid-state NMR and molecular modeling. *J. Phys. Chem. B* **2013**, *117*, 11292−11298.
(48) Megow, J.; Röhr, M. I. S.; Schmidt am Busch, M.; Renger, T.; Mitrić, R.; Kirstein, S.; Rabe, J. P.; May, V. Site-dependence of van der Waals interaction explains exciton spectra of double-walled tubular J-aggregates. *Phys. Chem. Chem. Phys.* **2015**, *17*, 6741−6747.
(49) Haverkort, F.; Stradomska, A.; de Vries, A. H.; Knoester, J. Investigating the structure of aggregates of an amphiphilic cyanine dye with molecular dynamics simulations. *J. Phys. Chem. B* **2013**, *117*, 5857−5867.
(50) Yu, Z.; Li, P.; Merz, K. M. Extended Zinc AMBER Force Field (EZAFF). *J. Chem. Theory Comput.* **2018**, *14*, 242−254.
(51) Holzwarth, A. R.; Schaffner, K. On the structure of bacteriochlorophyll molecular aggregates in the chlorosomes of green bacteria. A molecular modelling study. *Photosynth. Res.* **1994**, *41*, 225−233.
(52) Elstner, M.; Cui, Q.; Munih, P.; Kaxiras, E.; Frauenheim, T.; Karplus, M. Modeling zinc in biomolecules with the self consistent charge-density functional tight binding (SCC-DFTB) method: applications to structural and energetic analysis. *J. Comput. Chem.* **2003**, *24*, 565−581.
(53) Bystrova, M. I.; Mal'gosheva, I. N.; Krasnovskiĭ, A. A. Molecular mechanism of self-assembly of aggregated Molecular mechanism of self-assembly of aggregated bacteriochlorophyll c. *Molek. Biol.* **1979**, *13*, 582−594.
(54) Smith, K. M.; Kehres, L. A.; Fajer, J. Aggregation of the bacteriochlorophylls c, d, and e. Models for the antenna chlorophylls of green and brown photosynthetic bacteria. *J. Am. Chem. Soc.* **1983**, *105*, 1387−1389.
(55) Stewart, J. J. P. Optimization of parameters for semiempirical methods V: modification of NDDO approximations and application to 70 elements. *J. Mol. Model.* **2007**, *13*, 1173−1213.
(56) Stewart, J. J. P. *MOPAC*; 2016.
(57) Gaus, M.; Lu, X.; Elstner, M.; Cui, Q. Parameterization of DFTB3/3OB for Sulfur and Phosphorus for Chemical and Biological Applications. *J. Chem. Theory Comput.* **2014**, *10*, 1518−1537.
(58) Kubillus, M.; Kubař, T.; Gaus, M.; Řezáč, J.; Elstner, M. Parameterization of the DFTB3 method for Br, Ca, Cl, F, I, K, and Na in organic and biological systems. *J. Chem. Theory Comput.* **2015**, *11*, 332−342.
(59) Gaus, M.; Goez, A.; Elstner, M. Parametrization and Benchmark of DFTB3 for Organic Molecules. *J. Chem. Theory Comput.* **2013**, *9*, 338−354.
(60) Lu, X.; Gaus, M.; Elstner, M.; Cui, Q. Parametrization of DFTB3/3OB for magnesium and zinc for chemical and biological applications. *J. Phys. Chem. B* **2015**, *119*, 1062−1082.
(61) Grimme, S.; Ehrlich, S.; Goerigk, L. Effect of the damping function in dispersion corrected density functional theory. *J. Comput. Chem.* **2011**, *32*, 1456−1465.
(62) Aradi, B.; Hourahine, B.; Frauenheim, T. DFTB+, a sparse matrix-based implementation of the DFTB method. *J. Phys. Chem. A* **2007**, *111*, 5678−5684.
(63) *Matlab 2017b*, MATLAB and Statistics Toolbox release 2017b; 2017.

DOI: 10.1021/acs.jpclett.9b00303
J. Phys. Chem. Lett. 2019, 10, 2715−2724